THE JOURNAL OF PHYSICAL CHEMISTRY C

Article

pubs.acs.org/JPCC

Swelling Properties of Montmorillonite and Beidellite Clay Minerals from Molecular Simulation: Comparison of Temperature, Interlayer Cation, and Charge Location Effects

Stephanie L. Teich-McGoldrick,[†] Jeffery A. Greathouse,[*,†] Carlos F. Jové-Colón,[‡] and Randall T. Cygan[†]

[†]Geochemistry Department and [‡]Nuclear Waste Disposal Research and Analysis Department, Sandia National Laboratories, Albuquerque, New Mexico 87185, United States

Supporting Information

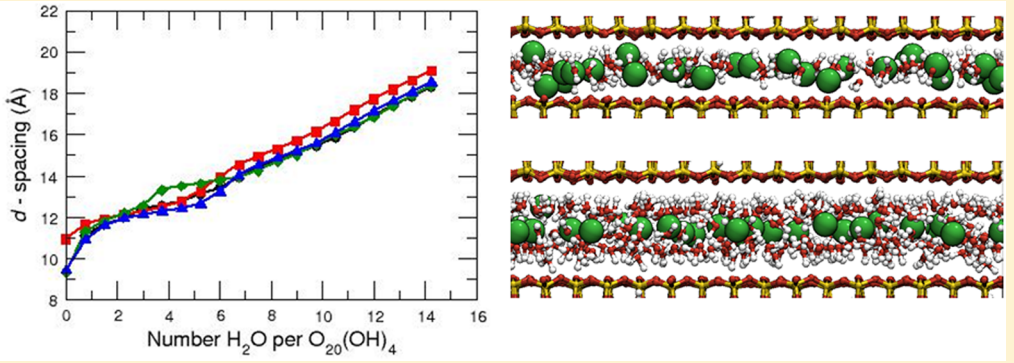

ABSTRACT: The swelling properties of smectite clay minerals are relevant to many engineering applications including environmental remediation, repository design for nuclear waste disposal, borehole stability in drilling operations, and additives for numerous industrial processes and commercial products. We used molecular dynamics and grand canonical Monte Carlo simulations to study the effects of layer charge location, interlayer cation, and temperature on intracrystalline swelling of montmorillonite and beidellite clay minerals. For a beidellite model with layer charge exclusively in the tetrahedral sheet, strong ion−surface interactions shift the onset of the two-layer hydrate to higher water contents. In contrast, for a montmorillonite model with layer charge exclusively in the octahedral sheet, weaker ion−surface interactions result in the formation of fully hydrated ions (two-layer hydrate) at much lower water contents. Clay hydration enthalpies and interlayer atomic density profiles are consistent with the swelling results. Water adsorption isotherms from grand canonical Monte Carlo simulations are used to relate interlayer hydration states to relative humidity, in good agreement with experimental findings.

Downloaded by SANDIA NATL LABORATORIES on September 13, 2015 | http://pubs.acs.org
Publication Date (Web): August 27, 2015 | doi: 10.1021/acs.jpcc.5b03253

INTRODUCTION

Smectites are abundant, naturally occurring clay minerals that readily swell in the presence of water. In addition to waste repository site selection, understanding the swelling process is relevant to many environmental and industrial processes. Clays play an important role in limiting the transport of hazardous contaminants in the subsurface.[1−3] They are also used commercially in cosmetics, pharmaceuticals, and construction materials and as catalysts.[4−8] The swelling properties of clay phases also contribute to their use as engineered barriers in nuclear waste repositories[9−12] and for preserving borehole stability during drilling during oil and gas production.[13] In particular, smectite clay is a key component of the engineered barrier system (EBS) considered in the disposition of high level nuclear waste in geological environments. The performance of EBS design concepts as a result of near-field geochemical interactions with barrier materials, including the host−rock natural barrier, are key to the long-term safety assessment of deep geological repositories.[14−16] Of particular importance is the disposition of heat-generating nuclear waste in canister configurations that could result in elevated temperature scenarios (e.g., in excess of 100 °C). Therefore, the response of swelling clay material to temperatures above ambient in the presence of fluids is important to long-term EBS performance.[15,17]

A repository for disposition of nuclear waste depends on several scientific factors, including how the local geological material will respond mechanically to changes in humidity and temperature. Due in part to the relatively high adsorptive capacity of smectite clay phases, repository sites can include clay-based shale formations with the use of smectite clay as an engineered backfill material surrounding the emplaced waste packages. A molecular-level understanding of the swelling and mechanical properties of smectite clays—and the effect of humidity and temperature—are needed to evaluate the basis for

Received: April 3, 2015
Revised: August 7, 2015
Published: August 27, 2015

© 2015 American Chemical Society

DOI: 10.1021/acs.jpcc.5b03253
J. Phys. Chem. C 2015, 119, 20880−20891

Downloaded by SANDIA NATL LABORATORIES on September 13, 2015 | http://pubs.acs.org
Publication Date (Web): August 27, 2015 | doi: 10.1021/acs.jpcc.5b03253

thermal limits and the resulting isolation performance of engineered and natural clay barriers.

Smectite clays are a natural product of the weathering and decomposition of igneous rocks.[18] Formed in a "T−O−T" layered pattern made from tetrahedral (T) silicate sheets surrounding octahedral (O) aluminum sheets, smectite clay layers are approximately 10 Å think. Isomorphic substitutions can occur in either the tetrahedral or octahedral sheets, resulting in a net negative charge that is balanced by hydrated cations located in the interlayer region. The interaction between negatively charged clay layers and positively charged interlayer cations controls the formation of nanosized clay platelets consisting of 10^1 -10^3 clay layers. Interlayer cations readily adsorb surrounding water, and because of the limited layer charge, smectite minerals can easily swell with the influx of water into the interlayer.

Several factors influence the swelling properties of smectite minerals. Thermodynamic variables include temperature,[19] external pressure,[20] humidity (water chemical potential),[21] and solution composition (osmotic pressure)[13] whereas structural variables include layer charge,[22] charge location,[23,24] and interlayer cation.[21,25] However, the high degree of disorder in these clay phases and small particle sizes have limited the use of experimental methods to definitively quantify these variables. Only recently has X-ray diffraction (XRD) profile modeling been used to correlate smectite swelling properties with layer charge location, cation species, and temperature.[19,26−29]

Computer simulation also offers the ability to investigate clay swelling properties at the molecular scale. Previously reported simulation data investigating the effect of layer charge location on clay swelling is limited, and the conclusions that can be drawn are varied. For example, Liu et al. reported that basal *d*-spacing increased for three different water contents as the large charge was shifted from the octahedral layers to the tetrahedral layers.[24] However, their data showed no significant trend within the reported error. Chávez-Páez et al. reported smaller values for an Otay montmorillonite, in which the layer charge was entirely localized to the octahedral layer, as compared to a Wyoming montmorillonite, in which a quarter of the layer charge was shifted from the octahedral to the tetrahedral sheets.[30] However, the charge density varied between the two different samples. Skipper et al. reported that the basal spacing increases with increasing tetrahedral charge layer for a Na-montmorillonite.[31] They attributed this behavior to the counterions binding directly above the tetrahedral charge sites in an inner-sphere complex. Although beyond the scope of this study, future work might focus on determining the stable swelling states from free energies, similar to published work,[32,33] using a narrow step size between water contents to help refine the data and conclusions.

In this study, we investigate the influence of temperature, cation species, and layer charge location on the crystalline swelling of smectite clays. Using molecular dynamics (MD) and grand canonical Monte Carlo (GCMC) simulations, the swelling states of Na-, Cs-, Ca-, and Mg-montmorillonite and beidellite clays were investigated at 298 and 425 K. These smectite compositions represent end-member cases in which the layer charge is located exclusively in either the octahedral sheet (montmorillonite) or the tetrahedral sheet (beidellite). First, we present trends in d_{001} (*d*-spacing) values for dry clay (0W), one-layer (1W), and two-layer (2W) hydrates as a function of cation species, layer charge location, and temperature. Interlayer compositions for the two smectite minerals represent the variation in charge, size, and hydration enthalpies expected for interlayer cations. One-dimensional density profiles are presented to provide a molecular-level description of the different swelling states. Finally, we provide a correlation between relative humidity (RH) and smectite swelling states. Though many studies have used MD simulation to calculate basal *d*-spacings at fixed water content, we also use GCMC simulations with variable water content to determine RH values corresponding to the formation of 2W hydrates. Thus, our approach provides a unique link to aid in the interpretation of clay swelling experiments.

MODEL AND METHODS

Molecular Dynamics Simulations. The model systems represent end members in both layer charge location and cation hydration enthalpy. Both smectite models have a layer charge of -0.75 $e{\cdot}uc^{-1}$ (e is the elementary charge, uc is the $O_{20}(OH)_4$-based unit cell) contained exclusively in the octahedral (montmorillonite) or tetrahedral (beidellite) sheets. The general chemical formula for the Na-montmorillonite model used in this work can be expressed as $Na_{0.75}Si_8$ $[Mg_{0.75}Al_{3.25}]$-$O_{20}(OH)_4{\cdot}nH_2O$, whereas the chemical formula for Na-beidellite can be expressed as $Na_{0.75}[Si_{7.25}A_{0.75}]$ $Al_4O_{20}(OH)_4{\cdot}$ nH_2O (brackets denote atoms in the octahedral and tetrahedral sheets for montmorillonite and beidellite, respectively). A representative snapshot of the Na-montmorillonite model is shown in Figure 1.

The simulation supercell consists of five orthogonal clay layers generated from the pyrophyllite crystal structure,[34] each containing 40 unit cells in an 8 × 5 expansion, with water contents ranging from dry clay to 14.25 $H_2O{\cdot}uc^{-1}$. Typical lateral dimensions (x, y) for the 8 × 5 × 5 supercells under dry conditions were approximately 41.5 and 45.0 Å for x and y, respectively. These x and y dimensions are within 0.1 Å of the a and b dimensions reported for a unit cell of pyrophyllite using Clayff,[35] indicating that the lateral dimensions of our clay models are sufficiently converged. Water content was increased in increments of 0.75 $H_2O{\cdot}uc^{-1}$. Negative layer charge was created by substituting Mg for Al in the octahedral sheet (montmorillonite) or Al for Si in the tetrahedral sheet (beidellite). Ten different charge configurations were created for each phase, with the charge sites randomly distributed throughout each layer subject to Lowenstein's substitution rule (i.e., substitution sites cannot be adjacent to each other).[36] The model configuration with the lowest potential energy was chosen for the subsequent simulations. For the final montmorillonite supercell model, the potential energy difference between the lowest energy and highest energy configurations is 165 $kJ{\cdot}mol^{-1}$, well above thermal energy at either 300 or 425 K. Further, because only adsorbed water is lost in hydrated smectites up to 200 °C (473 K),[37] we are confident that our supercell models are appropriate for the range of temperatures included in this study.

Interatomic potential energy terms included van der Waals and electrostatic atomic interactions taken from Clayff.[35] Clayff is an established classical force field successfully used in a wide range of mineral and environmental applications including the accurate modeling of structure, thermodynamics, spectroscopy, physical properties, adsorption, and transport behavior of minerals and other environmental phases.[38−42] Clayff is particularly appropriate for this study in elucidating the effects of substitution sites because the partial charges of oxygen atoms coordinating lattice cations (Si, Al, Mg) depend on the local

DOI: 10.1021/acs.jpcc.5b03253
J. Phys. Chem. C 2015, 119, 20880−20891

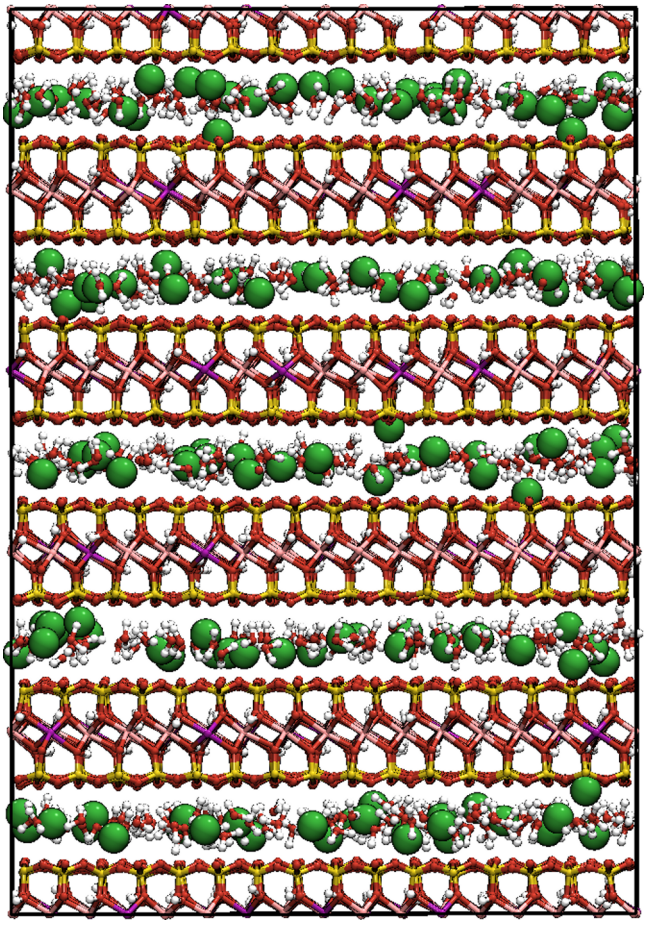

Figure 1. Equilibrium snapshot (*ac* plane) from MD simulation at 298 K at 1 atm of the Na-montmorillonite simulation supercell containing 210 water molecules in each of the five clay interlayers. Atoms are colored as follows: Mg, purple; Na, green; Si, yellow; O, red; H, white; Al, pink.

charge substitution pattern. The flexible SPC water model of Teleman et al. was used in conjunction with Clayff.[43]

Molecular dynamics simulations were performed using the LAMMPS[44] simulation package in the isobaric−isothermal ensemble (number of particles N, constant pressure P set to 1 atm, temperature T) and temperatures of 298 and 425 K. A Nosé−Hoover thermostat and barostat were used to control the pressure (independently in the x, y, and z directions) and the temperature.[45−48] The coupling constants for the barostat and thermostat were 100 and 1000 time steps, respectively. A time step of 0.5 fs was used, and periodic boundary conditions were applied in all directions. Short-range interactions were truncated at 10 Å, and long-range electrostatics were computed with the particle−particle particle-mesh solver and an accuracy of 1×10^{-4}.

Independent MD simulations were performed for each water content, cation, and clay species. Simulations were initialized with cations located in the midplane of the interlayer near charge substitution sites, and waters were inserted above and below the cation layer.[49] Random interlayer configurations were generated in the canonical (NVT) ensemble (volume V) with clay layers and interlayer cations fixed at their initial coordinates while allowing water molecules to freely move. The thermostat temperature was initially increased from 298 to 1000 K over 100 ps. Cations and water molecules were then allowed to move in a 100 ps stage at 1000 K, followed by a 100 ps stage in which the temperature was decreased to either 298 or 425 K. Finally, all atoms were allowed to move, and systems were equilibrated in the NPT ensemble for 1 ns. Potential energy and atomic position data were subsequently collected over 3 ns to obtain thermodynamic and structural properties. Structural data were collected every 50 ps, and thermodynamic data were collected every 0.5 ps.

The change in potential energy $\Delta U(N)$ associated with adding water molecules to a dry clay was calculated as a function of increasing water content:

$$\Delta U(N) = \frac{\langle U(N)\rangle - \langle U(0)\rangle}{N} \quad (1)$$

where $\langle U(N)\rangle$ is the average potential energy of the clay−water system containing N water molecules and $\langle U(0)\rangle$ is the average potential energy of the dry clay system.

GCMC Simulations. Water adsorption isotherms at 300 K were obtained from GCMC simulations using the Towhee code[50] in the grand canonical ensemble (μVT), where μ is the chemical potential of water. Model systems consisted of $4 \times 4 \times 2$ supercells of M-montmorillonite and M-beidellite (M = Na, Cs, Ca, Mg) as described above. Initial configurations of the clay layers were obtained from energy minimization of the dry clays, and layer atoms remained fixed at these coordinates during the subsequent GCMC simulations. Although this is an approximation relative to the MD simulations, maintaining fixed coordinates for clay layer atoms greatly improves the efficiency of these expensive simulations. Other than layer hydroxyl groups, whose positions can fluctuate within the layer, MD simulations indicate that atoms on the siloxane surfaces are generally immobile at aqueous interfaces.[51] Likewise, water molecules were treated as rigid bodies using the SPC\E model.[52] Values of the water chemical potential were related to relative humidity (P/P_0) on the basis of the saturation chemical potential, defined as the chemical potential (pressure) of a gas in equilibrium with the pure liquid. This value for SPC\E water at 300 K has been determined from GCMC simulation (−49.0 kJ·mol^{-1}).[53] Treating the water vapor as an ideal gas, values of μ can then be directly calculated from the RH,[54]

$$\mu = k_B T \ln \Lambda^3 \rho \quad (2)$$

where k_B is the Boltzmann constant, Λ is the thermal wavelength, and ρ is the density of the ideal gas.

Two basal d-spacing values were chosen for all clay models, corresponding to the 1W hydrate (12.0 Å) as observed in the MD swelling curves, and an expanded state at slightly larger d-spacing (15.0 Å) than any of the 2W states. Molecular models were also created corresponding to plateau regions in the MD swelling curves for Mg (13.5 Å) and Ca (14.5 Å) compositions, as discussed below. Interlayer cations were initially placed in the midplane between clay layers directly above (below) layer charge sites. As in the MD simulations, short-range interactions were truncated at 10 Å, and long-range electrostatics were computed using Ewald summation with an accuracy of 1.0×10^{-4}. GCMC moves were made according to the following probabilities: 40% configurational-bias insertion or deletion, 15% intrabox configurational-bias molecule transfer, 15% molecule regrowth, 15% center-of-mass translation, and 15% rotation about the center of mass. Only moves involving water molecules were allowed for the first 2.5×10^7 steps to allow the water molecules to equilibrate in the accessible interlayer

Downloaded by SANDIA NATL LABORATORIES on September 13, 2015 | http://pubs.acs.org
Publication Date (Web): August 27, 2015 | doi: 10.1021/acs.jpcc.5b03253

DOI: 10.1021/acs.jpcc.5b03253
J. Phys. Chem. C 2015, 119, 20880−20891

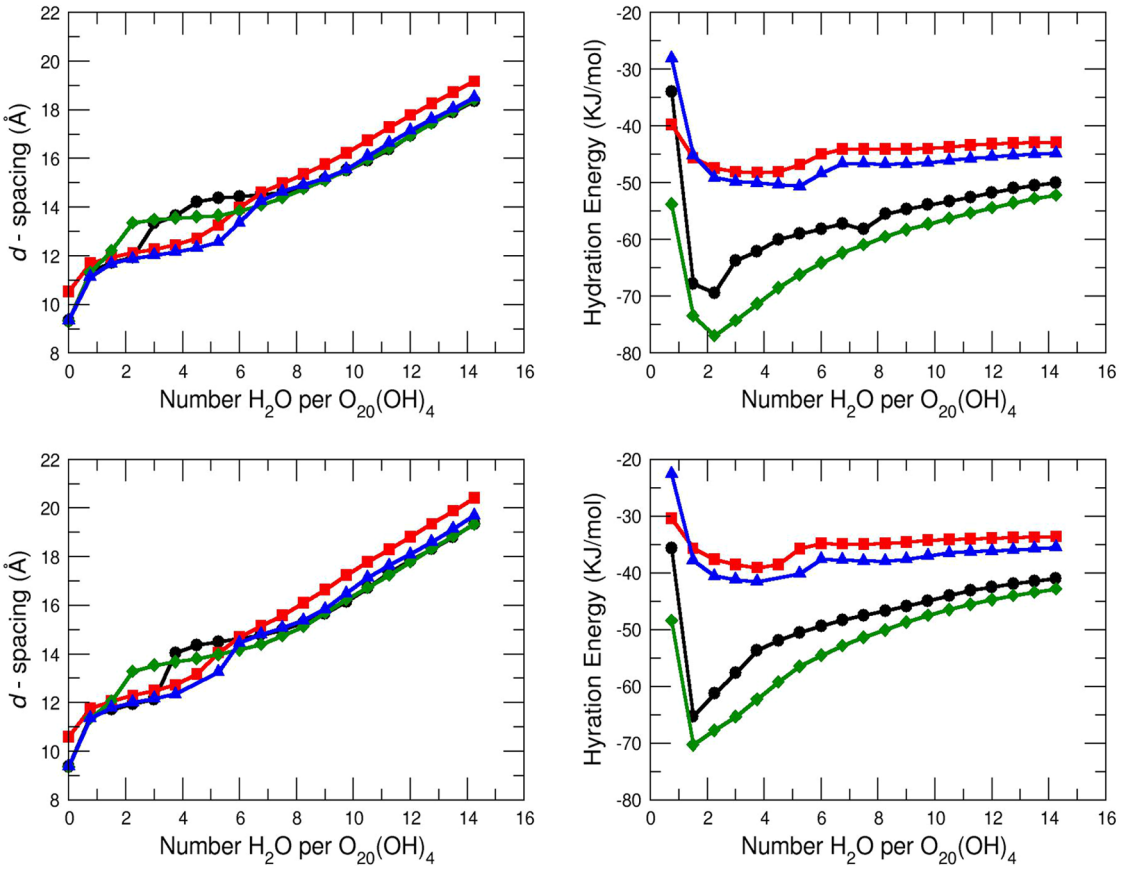

Figure 2. Montmorillonite swelling (basal *d*-spacing) curves (left) and hydration energies (right) as a function of water content from MD simulations at 1 atm and 298 K (top) and 425 K (bottom). Cations are identified as follows: Ca^{2+}, black circles; Cs^{+}, red squares; Mg^{2+}, green diamonds; Na^{+}, blue triangles. Error bars are smaller than symbols.

Table 1. Values of Basal *d*-Spacing (Å) from MD Simulations at 298 K and 1 atm for Montmorillonite and Beidellite as a Function of Interlayer Cation Compared with Previous Simulation and Experiment

		0W		1W		2W	
		this work	exp	this work	exp	this work	exp
Na^{+}	mont	9.35	9.6–9.8[21,58–61]	12.17	12.3–12.6[21,55,58]	14.91	14.9–15.6[21,55,58,59,61]
	beid	9.42	9.6–9.8[a,b,c]	12.26	12.4–12.5[a,b,c],		15.2–15.4[a]
Cs^{+}	mont	10.53	10.7–11.2[21,58–61]	12.28	11.9–12.6[58–60]		
	beid	10.93		12.27			
Ca^{2+}	mont	9.35		11.95		14.61	15.4–16.0[21,62,63]
	beid	9.32		11.94	11.78[d]		15.50[b]
Mg^{2+}	mont	9.30				13.61	13.9–14.9[64,65]
	beid	9.30		12.17		13.51	

[a]Experimental results for synthetic Na-saponite, a trioctahedral clay mineral with layer charge exclusively in the tetrahedral sheet.[24] [b]Experimental results at 0%, 30–60%, 100% RH for natural beidellites.[66] [c]Experimental results for natural Na-beidellite (Rupsroth, Germany).[67,68] [d]*d*-spacing value similar to that for a 1W layer on hydrated Mg-vermiculite.[66]

Table 2. Experimental Ion Radii and Hydration Enthalpies, and Water Contents ($H_2O{\cdot}uc^{-1}$) for 1W and 2W States in Montmorillonite and Beidellite from MD Simulations at 1 atm and 298 K

			1W[b]		2W[b]	
	radius[a] (Å)	$-\Delta H_{hyd}$[a] ($kJ{\cdot}mol^{-1}$)	mont	beid	mont	beid
Na^{+}	1.16	406	3.75 (5.00)	3.75 (5.00)	8.25 (11.00)	
Cs^{+}	1.81	276	3.00 (4.00)	3.00 (4.00)		
Ca^{2+}	1.14	1577	2.25 (6.00)	2.25 (6.00)	7.5 (20.00)	
Mg^{2+}	0.86	1921		2.25 (6.00)	4.5 (12.00)	4.5 (12.00)

[a]Ionic radii and hydration enthalpies (ΔH_{hyd}) are shown for ref 3. [b]Values in parentheses correspond to water content in $H_2O{\cdot}cation^{-1}$.

Downloaded by SANDIA NATL LABORATORIES on September 13, 2015 | http://pubs.acs.org
Publication Date (Web): August 27, 2015 | doi: 10.1021/acs.jpcc.5b03253

DOI: 10.1021/acs.jpcc.5b03253
J. Phys. Chem. C 2015, 119, 20880–20891

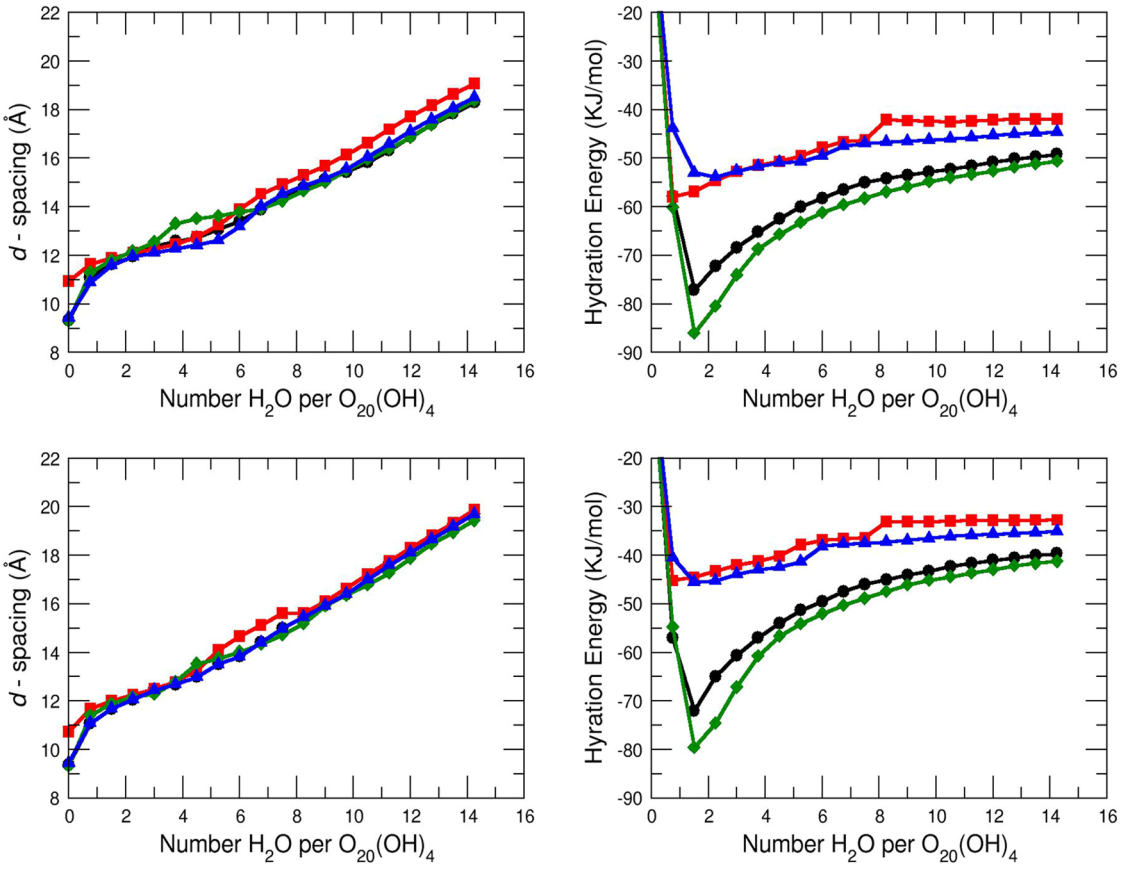

Figure 3. Beidellite swelling curves (left) and hydration energy (right) as a function of water content from MD simulations at 1 atm and T = 298 K (top) and 425 K (bottom). Cations are identified as follows: Ca^{2+}, black circles; Cs^{+}, red squares; Mg^{2+}, green diamonds; Na^{+}, blue triangles. Error bars are smaller than symbols.

region. For the remaining 7.5×10^7 steps, translation moves of interlayer cations were also included with a 10% relative probability (90% of the translation moves involved water molecules). Configurations and energies were stored over the final 5.0×10^7 steps for subsequent energy and structure analysis.

RESULTS AND DISCUSSION

Swelling Curves. The swelling and hydration energy curves for the montmorillonite models at 298 and 425 K are shown in Figure 2. Standard deviations for both the basal d-spacing and hydration energies were calculated from block averaging; uncertainties in the data are less than the symbol size. The overall stepwise swelling behavior of montmorillonite agrees well with previous simulations and experimental studies, confirming that the interlayer cation has an important effect on clay swelling.[21,25,55−57] For each cation, the 1W and 2W states are identified on the basis of the location of plateaus in the swelling curves. The associated values of the d-spacing are compared with available experimental data in Table 1, and the water contents in units of $H_2O{\cdot}uc^{-1}$ are given in Table 2.

Comparing the swelling curves for monovalent cesium and sodium cations, one clearly sees that Cs-montmorillonite has an expanded interlayer space compared to that for Na-montmorillonite. This result is consistent with cesium having a larger ionic radius than sodium (1.84 Å compared to 1.16 Å).[69] Na-montmorillonite shows distinct 0W−1W and 1W−2W transitions, although the 2W state is less obvious than 1W and has a slight increase in d-spacing as the water content increases. In fact, the 2W plateau region for Na-montmorillonite (7.5−9.0 $H_2O{\cdot}uc^{-1}$) has only a slightly smaller slope than the expanded region at higher water content. In contrast, only the 0W−1W transition is observed in Cs-montmorillonite, suggesting that this smectite composition does not expand beyond the 1W state.

In general, the simulated basal d-spacings for montmorillonite agree well with previously published experimental data (Table 1), and they are consistent with previous simulation results for montmorillonites with interlayer monovalent ions.[24,25,49,56,70−74] It should be noted that the previous studies represent a range of charge site locations and charge densities. Cs-montmorillonite does not expand to form a 2W state in nature,[58,61] and our MD results show a gradual expansion of the interlayer without the formation of a stable 2W state. Na-montmorillonite has been observed to form a three-layer hydrate at higher water content, but we did not investigate these systems in this work.

Model smectite systems with divalent cations expand at lower water content than those with monovalent cations; this is consistent with predicted behavior on the basis of cation hydration energies (Table 2).[21,74] Experimentally, Mg- and Ca-montmorillonite are known to form only two-layer hydrates.[19] As illustrated in Figure 2, there is a distinct plateau at the two-layer hydrate for Ca-montmorillonite and a smaller, less pronounced plateau at lower water concentrations. This virtual 1W state for Ca-montmorillonite has been observed previously in simulation[73] and corresponds to an interlayer spacing of 11.95 Å. The swelling curve for Mg-montmorillonite exhibits a

Downloaded by SANDIA NATL LABORATORIES on September 13, 2015 | http://pubs.acs.org
Publication Date (Web): August 27, 2015 | doi: 10.1021/acs.jpcc.5b03253

DOI: 10.1021/acs.jpcc.5b03253
J. Phys. Chem. C 2015, 119, 20880−20891

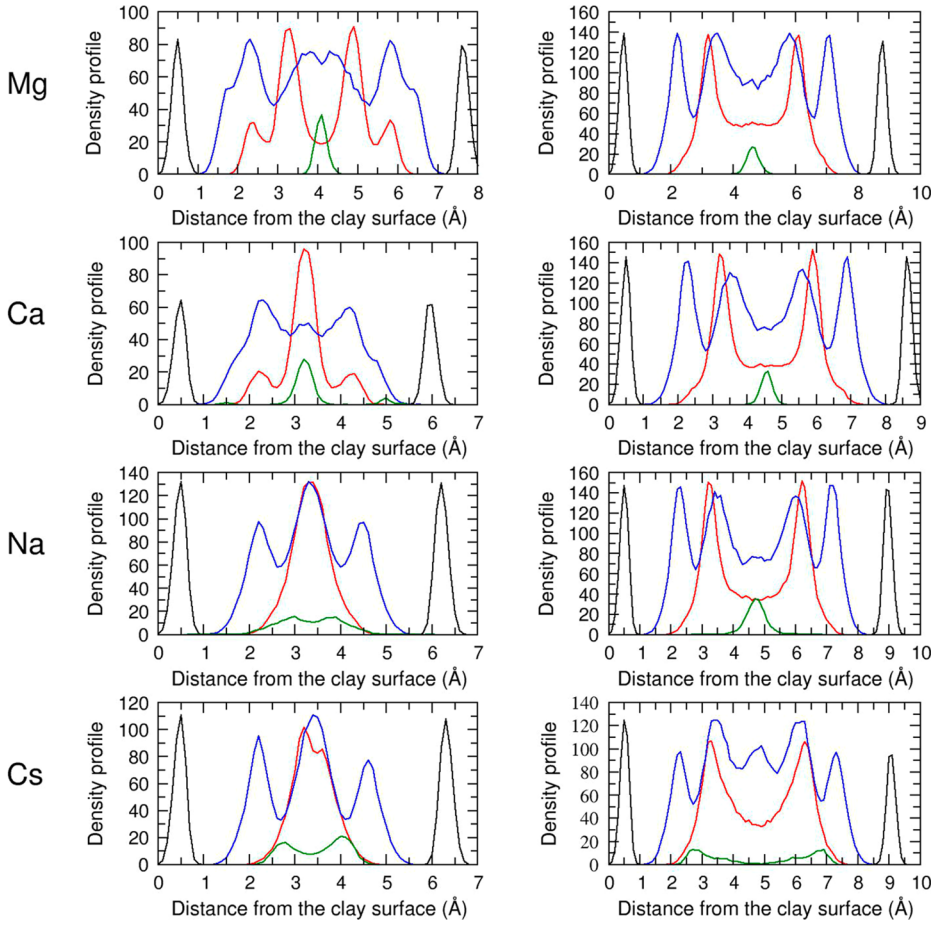

Figure 4. Atomic density profiles from MD simulations at 1 atm and 298 K for montmorillonite showing interlayer cation (green), water oxygen atoms (red), water hydrogen atoms (blue), and clay surface oxygen atoms (black). The density profiles correspond to the following water contents per clay unit cells in the left/right-hand columns: Cs^+, 3.00/7.50; Na^+, 3.75/8.25; Ca^{2+}, 2.25/7.50; Mg^{2+}, 4.50/9.00.

single plateau corresponding to a two-layer hydrate with a basal spacing of 13.61 Å. This expansion is slightly smaller than previously reported simulation data, 13.83 Å,[57] and experimental data, 13.9 and 14.85 Å.[64,65]

Trends in basal *d*-spacing for the beidellite models (Table 1 and Figure 3) show significant differences with montmorillonite, highlighting the effect of layer charge location in the tetrahedral sheet compared to that in the octahedral sheet. For the 0W and 1W states, *d*-spacing values for beidellite are larger than or approximately equal to that of montmorillonite. Only Mg-beidellite shows a distinct plateau in *d*-spacing corresponding to the 2W state. Na- and Cs-beidellite show a well-defined 1W state with a slightly flatter profile near 15.0 Å than the expanded region at higher water content. However, for the 2W state, the trend is reversed and the interlayer spacing for montmorillonite is larger than that observed by simulation for beidellite. These trends are consistent with *d*-spacings observed by Sato et al.[66] and Suquet et al.[67] for Na-saturated montmorillonite and beidellite as a function of relative humidity. Overall, the expansion of beidellite is considered to be intermediate between that of montmorillonite and vermiculite.[66] It should be noted that although there is good agreement between predicted and experimental *d*-spacings for beidellites, data values from experiments[66−68] pertain to natural samples that are not pure and to a certain extent tend to be mixed with other clays.

Potential Energies. The results for montmorillonite and beidellite are presented in Figures 2 and 3, respectively. At high water content, $\Delta U(N)$ approaches the internal energy of bulk SPC water, −41.4 kJ·mol^{-1}.[43] During the first stage of hydration for the monovalent cations, the energy drops significantly below the bulk water value. As hydration continues, this energy rises before leveling off. For the divalent cations, the hydration energy drops significantly below the value for the monovalent cations before continuously increasing with water content. In the first phase of hydration at low water content, the hydration energies for beidellite are up to 10 kJ·mol^{-1} lower than those for montmorillonite, showing that it is energetically more favorable to add a water molecule to a system with tetrahedral charge sites near the clay−water interface than to the charge sites associated with the octahedral sheet that is removed from the interface.

Temperature Effects. The effects of temperature on basal *d*-spacing can be seen in Figures 2 and 3. In general, increasing temperature results in increased *d*-spacing values due to the increased thermal motion of the interlayer species. This is consistent with the experimental work of Morodome and Kawamura on the swelling behavior of Na-montmorillonite.[19] For Na-montmorillonite, the swelling curves at both temperatures show distinct 1W−2W transitions at similar water contents. The shift to larger *d*-spacing values is most prominent in the transition regions and the least prominent in the 1W

Downloaded by SANDIA NATL LABORATORIES on September 13, 2015 | http://pubs.acs.org
Publication Date (Web): August 27, 2015 | doi: 10.1021/acs.jpcc.5b03253

DOI: 10.1021/acs.jpcc.5b03253
J. Phys. Chem. C 2015, 119, 20880−20891

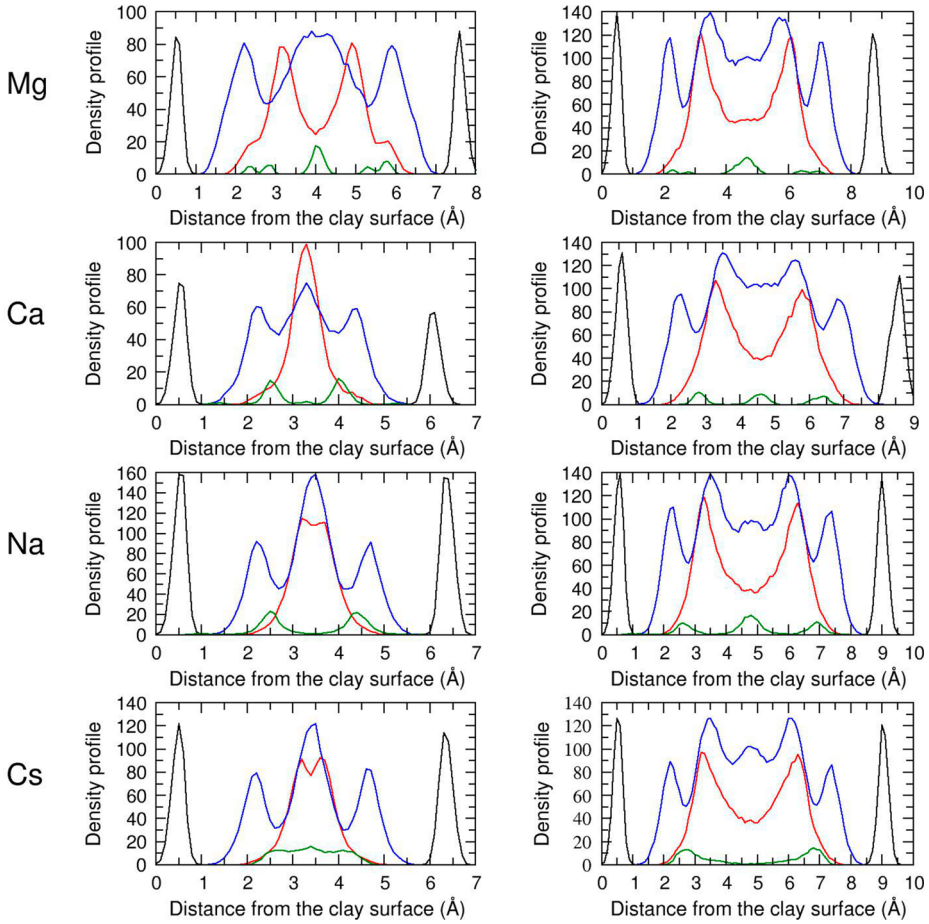

Figure 5. Atomic density profiles from MD simulations at 1 atm and 298 K for beidellite showing interlayer cation (green), water oxygen atoms (red), water hydrogen atoms (blue), and clay surface oxygen atoms (black). The density profiles correspond to the following water contents per clay unit cells in the left/right-hand columns: Cs^+, 3.00/7.50; Na^+, 3.75/8.25; Ca^{2+}, 2.25/7.50; Mg^{2+}, 4.50/8.25.

state. The swelling curves of Na-beidellite are similar; however, the 1W−2W transition is not seen at 425 K.

Interlayer Molecular Structure. For each cation−clay combination, the distributions of cations and water molecules in the interlayer were calculated for select hydration states and are shown as one-dimensional atomic density profiles in Figures 4 and 5. These profiles represent the average cation and water molecule locations across all five interlayers associated with the simulation supercell. For montmorillonite (Figure 4), the 1W and 2W interlayer structures are shown for sodium, cesium, and calcium ions. Magnesium profiles are shown at the initial formation of the 2W state (4.50 $H_2O{\cdot}uc^{-1}$) and at 8.25 $H_2O{\cdot}uc^{-1}$. Cesium ions remain close to the surface as the water content increases, rather than forming a single layer at the interlayer midplane. At both low and high water content, the cesium distribution forms two peaks approximately 2.2 Å from the surface oxygen atoms. No water molecules are interposed between cesium ions and the surface, indicating inner-sphere adsorption. Sodium ions in the 1W state form a broad peak with maxima near each clay surface. As the water content increases and a two-layer hydrate forms, sodium ions form a single peak at the midplane consistent with an outer-sphere surface complex. The calcium profile in the 1W state consists of a large peak at the midplane (inner-sphere complex) and two minor peaks approximately 1.0 Å from surface oxygen atoms, previously described as "anhydrous" due to their unusual adsorption within ditrigonal cavities on the basal surface.[75] These same anhydrous ions are faintly visible in the 1W state of Ca-beidellite (Figure 5). In the 2W state, calcium ions form a single peak at the midplane of the interlayer (outer-sphere surface complex). The magnesium profile at lower water content shows a single cation peak at the midplane and a splitting of the water oxygen distribution into four peaks. The outer water peaks are also present in the calcium 1W profile and correspond to water molecules forming strong hydrogen bonds with the surface. At a higher water content that corresponds to a *d*-spacing of 15.1 Å, only two water layers are seen, consistent with the 2W interlayer structures for the Na and Ca cases.

Comparing the montmorillonite density profiles with those for beidellite (Figure 5), it is clear that layer charge location has a strong effect on interlayer structure for both cation and water. Cations in the beidellite interlayer tend to remain closer to the clay surface at higher water contents than in the montmorillonite interlayer. In the 1W state of beidellite, for example, the interlayer sodium ions form two distinct peaks corresponding to surface adsorption compared to the broad centered profile seen in the montmorillonite interlayer. In the 2W state, sodium ions split to form three peaks in the beidellite interlayer, indicating both outer-sphere and inner-sphere surface complexes, compared to the single peak in the montmorillonite interlayer (outer-sphere surface complex). The 2W beidellite density profiles for calcium and magnesium ions also show three peaks, despite the large hydration energies for these

Downloaded by SANDIA NATL LABORATORIES on September 13, 2015 | http://pubs.acs.org
Publication Date (Web): August 27, 2015 | doi: 10.1021/acs.jpcc.5b03253

DOI: 10.1021/acs.jpcc.5b03253
J. Phys. Chem. C 2015, 119, 20880−20891

divalent ions. Equilibrium snapshots from the 1W and 2W states of Na-montmorillonite and Na-beidellite are shown in Figure 6 and serve to illustrate the interlayer profiles discussed above.

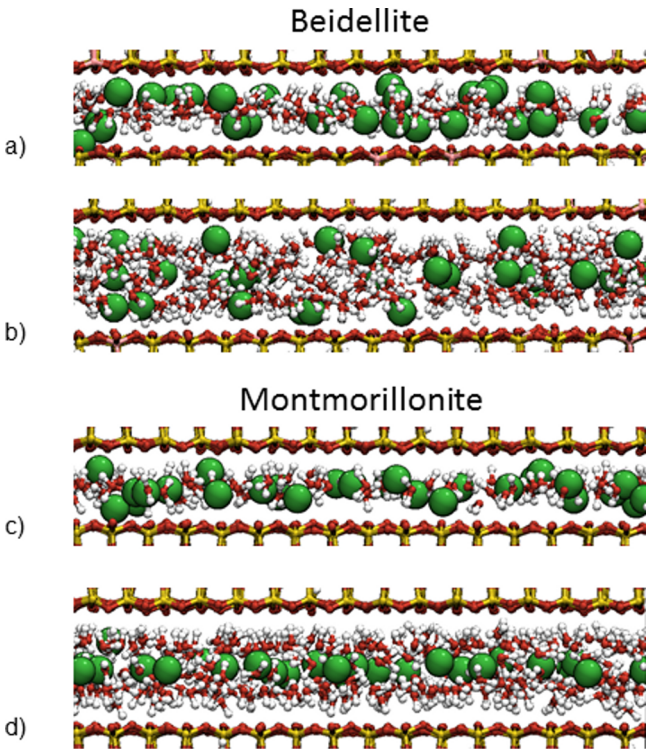

Figure 6. Equilibrium snapshots from MD simulations at 1 atm and 298 K corresponding to the density profiles for (a) 1W Na-beidellite, (b) 2W Na-beidellite, (c) 1W Na-montmorillonite, and (d) 2W Na-montmorillonite. The color scheme is the same as in Figure 1.

GCMC Simulations. Simulations in the μVT ensemble were performed to determine water content in the interlayers at *d*-spacings corresponding to plateau regions in the simulated swelling curves (Figures 2-3, MD simulations in the *NPT* ensemble). Note that neither ensemble (μVT or *NPT*) can independently determine the thermodynamically stable swelling states under laboratory conditions (i.e., fixed temperature, pressure, and relative humidity). Swelling states can be examined in more detail using a combination of molecular simulation and osmotic framework adsorbed solution theory,[76] but such calculations are beyond the scope of the present work.

Water adsorption isotherms from the GCMC simulations are shown in Figures S1−S4 in the Supporting Information. Adsorption loadings are given in units of water molecules per unit cell ($H_2O{\cdot}uc^{-1}$) for consistency with the MD swelling curves (Figures 2 and 3). Isotherms for the Na-clays are consistent with published results for Na-montmorillonite from GCMC simulations[20,77] and experiment.[27] Atomic density profiles of interlayer ions and water molecules for basal *d*-spacing values of 12.0 and 15.0 Å (data not shown) are consistent with the MD results (Figures 4 and 5) and are representative of 1W and 2W states, respectively. The initial water uptake corresponds to ion hydration,[20] followed by a gradual increase in adsorbed water until a maximum loading is reached. For each ion, the maximum loadings (Table 3) are similar for montmorillonite and beidellite, indicating little dependence on location of layer charge. For both the 12.0 and 15.0 Å states, the maximum loading correlates with ion hydration enthalpy, and there is some dependence on ionic radius within each pair of monovalent and divalent cations. Clay interlayers containing the smaller divalent ions with their large hydration energies can accommodate more water. Although sodium and calcium ions have nearly identical radii, the much smaller sodium hydration enthalpy results in a substantially lower water content for the 12.0 Å phase. Clays containing the large and weakly hydrating cesium ion have even fewer water molecules per interlayer.

Table 3. Maximum Loadings ($H_2O{\cdot}uc^{-1}$) from GCMC Simulations at 298 K at *d*-Spacing Values of 12.0 and 15.0 Å

	montmorillonite		beidellite	
interlayer ion	12.0 Å	15.0 Å	12.0 Å	15.0 Å
Na^+	4.3	9.0	4.0	9.1
Cs^+	3.7	8.0	3.6	8.2
Ca^{2+}	5.0	9.3 (8.5)[a]	5.0	9.5
Mg^{2+}	5.4	9.4 (7.2)[a]	5.4	9.7 (7.1)[a]

[a]Values in parentheses correspond to plateau regions in the MD swelling curves (14.5 Å for Ca-montmorillonite, 13.5 Å for Mg-montmorillonite, and Mg-beidellite).

For a basal *d*-spacing of 15.0 Å, the presence of outer-sphere surface complexes for Na-, Ca-, and Mg-smectites results in a consistent water content regardless of ion size or hydration enthalpy. The maximum loading for the Na-smectites is slightly lower than that of the divalent cations because a small fraction of sodium ions form inner-sphere surface complexes with the basal surfaces. Although a 15.0 Å phase is not seen experimentally for Cs-smectites, cesium ions form exclusively inner-sphere surface complexes, resulting in a lower water content than the other model systems. It should be noted that the maximum loadings in Table 3 correspond to the basal *d*-spacing values chosen for GCMC simulations, and these *d*-spacing values may not correspond to exact thermodynamic or mechanical equilibrium.

By comparing MD swelling curves with GCMC adsorption isotherms, we can assign approximate RH ranges to gravimetric water contents corresponding to plateau regions in the MD swelling curves (Figures 2 and 3). Water contents at specific RH values for 1W and 2W states are compared with experimental XRD profiling results for monovalent ions (Figure 7) and divalent ions (Figure 8). The 1W state (12.0 Å) is dominant at low RH, which is consistent with experimental findings for Na-saponite[27] and Na-montmorillonite.[78] For cations that are known to form 2W states (Na^+, Ca^{2+}, Mg^{2+}), Figures 7 and 8 indicate that these phases begin to form at lower RH values for Na^+ compared to the divalent ions. Specifically, the onset of the 2W state in Na-clays at RH 0.6−0.8 agrees well with experimentally determined values of approximately 0.50 and 0.60 for low-charge Na-saponite[27] and Na-montmorillonite,[78] respectively.

Interlayer expansion to form the 2W state occurs at much lower RH (0.15−0.45) for the Ca- and Mg-clays (Figure 8), which is consistent with the experimental observation of these same states at RH values between 0.20−0.40.[78] Although the water contents for Mg-montmorillonite closely match the experimental values for Mg-montmorillonite, results for Ca-montmorillonite overpredict the experimental values by 1.5−2.0 $H_2O{\cdot}uc^{-1}$ (4−5 $H_2O{\cdot}ion^{-1}$). Expansion of the interlayers containing Mg^{2+} and Ca^{2+} ions from their plateau *d*-spacing values (13.5 and 14.5 Å, respectively) to a slightly larger value

Downloaded by SANDIA NATL LABORATORIES on September 13, 2015 | http://pubs.acs.org
Publication Date (Web): August 27, 2015 | doi: 10.1021/acs.jpcc.5b03253

DOI: 10.1021/acs.jpcc.5b03253
J. Phys. Chem. C 2015, 119, 20880−20891

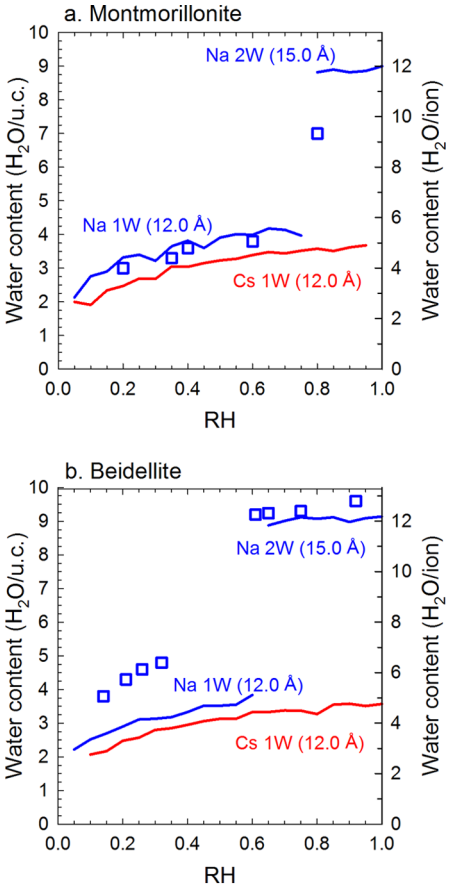

Figure 7. Comparison of water content and RH for 1W and 2W states for monovalent ions in (a) montmorillonite and (b) beidellite. Results from GCMC simulations at 298 K at the indicated basal *d*-spacings (solid lines) are compared with experimental data (open symbols) for montmorillonite[78] and Na-saponite.[27]

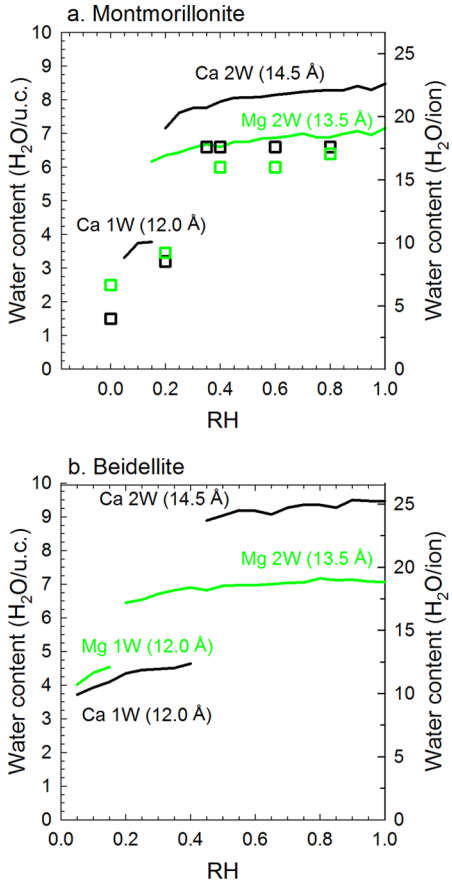

Figure 8. Comparison of water content and RH for 1W and 2W states for divalent ions in (a) montmorillonite and (b) beidellite. Results from GCMC simulations at 298 K at the indicated basal *d*-spacings (solid lines) are compared with experimental data (open symbols) for montmorillonite.[78]

commonly associated with 2W states (15.0 Å) results in a more uniform water content for all ions (Table 3), but the experimental XRD results clearly show that thermodynamically 2W states for each cation differ significantly in water content. Generally, predicted water contents for the 1W and 2W states of the montmorillonites are in good agreement with experiment, considering the limited amount of experimental data and differences in simulated smectite models compared with the SWy-1 used in the experiments.[78]

CONCLUSIONS

We have studied the effects of layer charge location, interlayer cation, and temperature on the swelling properties of smectite clays via MD and GCMC simulations. With molecular simulation, we are able to examine clay hydration phenomena on pure end member phases without the complications of disorder, poor crystallinity, and mixed charge or hydration states as observed in experiments. The montmorillonite and beidellite models investigated here have layer charge exclusively in the octahedral and tetrahedral sheets, respectively, to better isolate the effect of layer charge location on clay hydration properties. Including monovalent ions (Na^+, Cs^+) and divalent ions (Ca^{2+}, Mg^{2+}) in the interlayer spans a wide range of ionic radii and hydration enthalpies.

Simulated swelling curves for montmorillonite with different interlayer cations agree well with published data. The effect of ion hydration enthalpy on clay swelling is evident for the divalent ions, which form complete hydration shells at very low water content (2–4 $H_2O{\cdot}uc^{-1}$ for montmorillonite, 4–6 $H_2O{\cdot}uc^{-1}$ for beidellite). Full hydration of calcium and magnesium ions is accompanied by interlayer expansion to form the 2W state. We also find that layer charge location has a strong effect on interlayer structure. When tetrahedral charge sites are present (beidellite), ions remain adsorbed to the surface (inner-sphere surface complexes) at much higher water contents compared to montmorillonite. Magnesium has the largest hydration enthalpy in our models, yet inner-sphere magnesium surface complexes are observed in the beidellite interlayer in the 2W state. In montmorillonite, in which the octahedral layer charge is further removed from the interlayer and partially screened by atoms in the tetrahedral sheet, all ions studied except cesium are completely hydrated (outer-sphere surface complexes) in the 2W state. In general, increasing temperature from 298 to 425 K shifts the swelling curves to higher basal *d*-spacing values with very little difference in interlayer structure.

GCMC simulations were used to obtain water adsorption isotherms at basal *d*-spacing values corresponding to 1W and 2W states. The resulting isotherms were used to correlate RH values with water content from plateau regions from the MD swelling curves. Our assigned RH values and water contents for the 1W and 2W states in the model clays are consistent with experimental XRD profiling results.

Downloaded by SANDIA NATL LABORATORIES on September 13, 2015 | http://pubs.acs.org
Publication Date (Web): August 27, 2015 | doi: 10.1021/acs.jpcc.5b03253

DOI: 10.1021/acs.jpcc.5b03253
J. Phys. Chem. C 2015, 119, 20880–20891

It has been estimated that heat-generating radioactive waste emplaced in large canisters will produce temperatures well in excess of 100 °C.[79] As a potential follow-on application of this work, a consistent set of clay swelling and structural properties from molecular simulations at elevated temperatures could be used in the thermodynamic modeling of clay phases under conditions relevant to deep geological repositories. Therefore, exploiting molecular simulations, along with thermodynamic modeling and experimental investigations of clay hydrothermal interactions, can provide the scientific basis to advance thermal constraints in clay barriers within adequate compliance of the safety requirements.

■ ASSOCIATED CONTENT

Supporting Information

The Supporting Information is available free of charge on the ACS Publications website at DOI: 10.1021/acs.jpcc.5b03253.

Water adsorption isotherms from GCMC simulations at 300 K for montmorillonite and beidellite model systems (PDF)

■ AUTHOR INFORMATION

Corresponding Author

*J. A. Greathouse. E-mail: jagreat@sandia.gov.

Notes

The authors declare no competing financial interest.

■ ACKNOWLEDGMENTS

This work is supported by the U.S. Department of Energy, Used Fuel Disposition Campaign, and by the U.S. Department of Energy, Office of Basic Energy Sciences, Geosciences Research Program. Sandia National Laboratories is a multiprogram laboratory managed and operated by Sandia Corporation, a wholly owned subsidiary of Lockheed Martin Corporation, for the U.S. Department of Energy's National Nuclear Security Administration, under contract DE-AC04-94AL85000.

■ REFERENCES

(1) Yuan, G. D.; Theng, B. K. G.; Churchman, G. J.; Gates, W. P. Clays and Clay Minerals for Pollution Control. In *Handbook of Clay Science*, second ed.; Bergaya, F., Lagaly, G., Eds.; Elsevler: Amsterdam, 2013; Vol. *B*.

(2) Morrow, C. P.; Yazaydin, A. O.; Krishnan, M.; Bowers, G. M.; Kalinichev, A. G.; Kirkpatrick, R. J. Structure, Energetics, and Dynamics of Smectite Clay Interlayer Hydration: Molecular Dynamics and Metadynamics Investigation of Na-Hectorite. *J. Phys. Chem. C* **2013**, *117*, 5172−5187.

(3) *CRC Handbook of Chemistry and Physics*, 71st ed.; Lide, D. R., Ed.; CRC Press: Boca Raton, FL, 1990.

(4) Amato, I. Concrete Solutions. *Nature* **2013**, *494*, 300−301.

(5) Carretero, M. I. Clay Minerals and their Beneficial Effects upon Human Health. A Review. *Appl. Clay Sci.* **2002**, *21*, 155−163.

(6) Hanczyc, M. M.; Fujikawa, S. M.; Szostak, J. W. Experimental Models of Primitive Cellular Compartments: Encapsulation, Growth, and Division. *Science* **2003**, *302*, 618−622.

(7) Isabel Carretero, M.; Pozo, M. Clay and Non-Clay Minerals in the Pharmaceutical Industry Part I. Excipients and Medical Applications. *Appl. Clay Sci.* **2009**, *46*, 73−80.

(8) Macewan, D. M. C. Clay Minerals as Catalysts and Adsorbents. *Nature* **1948**, *162*, 195−196.

(9) Coulon, H.; Lajudie, A.; Debrabant, P.; Atabek, R.; Jorda, M.; Andre-Jehan, R. Choice of French Clays as Engineered Barrier Components for Waste Disposal. *Scientific Basis for Nuclear Waste Management X* **1987**, 813−824.

(10) Galle, C. Gas Migration and Breakthrough Pressure in a Compacted Clay for the Engineered Barrier of a Deep Disposal. *Bull. Soc. Geol. Fr.* **1998**, *169*, 675−680.

(11) Montes-H, G.; Marty, N.; Fritz, B.; Clement, A.; Michau, N. Modelling of Long-Term Diffusion-Reaction in a Bentonite Barrier for Radioactive Waste Confinement. *Appl. Clay Sci.* **2005**, *30*, 181−198.

(12) Zachara, J. M.; Serne, J.; Freshley, M.; Mann, F.; Anderson, F.; Wood, M.; Jones, T.; Myers, D. Geochemical Processes Controlling Migration of Tank Wastes in Hanford's Vadose Zone. *Vadose Zone J.* **2007**, *6*, 985−1003.

(13) Anderson, R. L.; Ratcliffe, I.; Greenwell, H. C.; Williams, P. A.; Cliffe, S.; Coveney, P. V. Clay Swelling - A Challenge in the Oilfield. *Earth-Sci. Rev.* **2010**, *98*, 201−216.

(14) Jové Colón, C. F.; Caporuscio, F. A.; Levy, S. S.; Blink, J. A.; Greenberg, H. R.; Halsey, W. G.; Fratoni, M.; Sutton, M.; Wolery, T. J.; Rutqvist, J.; Liu, H. H.; Birkholzer, J.; Steefel, C. I.; Galindez, J. *Disposal Systems Evaluations and Tool Development - Engineered Barrier System (EBS) Evaluation* **2011**, 1−192.

(15) Jové Colón, C. F.; Weck, P. F.; Sassani, D. C.; Zheng, L.; Rutqvist, J.; Steefel, C. I.; Kim, K.; Nakagawa, S.; Houseworth, J.; Birkholzer, J.; Caporuscio, F. A.; Cheshire, M.; Rearick, M. S.; McCarney, M. K.; Zavarin, M.; Benedicto-Cordoba, A.; Kersting, A. B.; Sutton, M.; Jerden, J. L.; Frey, K. E.; Copple, J. M.; Ebert, W. L. *Evaluation of Used Fuel Disposition in Clay-Bearing Rock (FCRD-UFD-2014-000056)*; SAND2014-18303 R; Sandia National Laboratories: Albuquerque, New Mexico, 2014; pp 434.

(16) Nutt, M.; Voegele, M.; Jove-Colon, C.; Wang, Y.; Howard, R.; Blink, J.; Liu, H.-H.; Hardin, E.; Jenni, K. *Used Fuel Disposition Campaign Disposal Research and Development Roadmap (FCR&D-USED-2011-000065)* **2011**, 1−138.

(17) Cheshire, M.; Caporuscio, F. A.; Rearick, M. S.; Jové Colón, C. F.; McCarney, M. K. Bentonite Evolution at Elevated Pressures and Temperatures: An Experimental Study for Generic Nuclear Repository Designs. *Am. Mineral.* **2014**, *99*, 1662−1675.

(18) Zoltai, T.; Stout, J. H. *Mineralogy Concepts and Principles*; Burgess Publishing Co.: 1984.

(19) Morodome, S.; Kawamura, K. Swelling Behavior of Na and Ca-Montmorillonite up to 150°C by in Situ X-ray Diffraction Experiments. *Clays Clay Miner.* **2009**, *57*, 150−160.

(20) Smith, D. E.; Wang, Y.; Chaturvedi, A.; Whitley, H. D. Molecular Simulations of the Pressure, Temperature, and Chemical Potential Dependencies of Clay Swelling. *J. Phys. Chem. B* **2006**, *110*, 20046−20054.

(21) Mooney, R. W.; Keenan, A. G.; Wood, L. A. Adsorption of Water Vapor by Montmorillonite. II. Effect of Exchangeable Ions and Lattice Swelling as Measured by X-Ray Diffraction. *J. Am. Chem. Soc.* **1952**, *74*, 1371−1374.

(22) Slade, P. G.; Quirk, J. P.; Norrish, K. Crystalline Swelling of Smectite Samples in Concentrated NaCl Solutions in Relation to Layer Charge. *Clays Clay Miner.* **1991**, *39*, 234−238.

(23) Greathouse, J.; Sposito, G. Monte Carlo and Molecular Dynamics Studies of Interlayer Structure in $Li(H_2O)_3$−Smectites. *J. Phys. Chem. B* **1998**, *102*, 2406−2414.

(24) Liu, X.; Lu, X.; Wang, R.; Zhou, H. Effects of Layer-Charge Distribution on the Thermodynamic and Microscopic Properties of Cs-smectite. *Geochim. Cosmochim. Acta* **2008**, *72*, 1837−1847.

(25) Boek, E. S.; Coveney, P. V.; Skipper, N. T. Monte Carlo Molecular Modeling Studies of Hydrated Li-, Na-, and K-Smectites: Understanding the Role of Potassium as a Clay Swelling Inhibitor. *J. Am. Chem. Soc.* **1995**, *117*, 12608−12617.

(26) Zachara, J. M.; Serne, J.; Freshley, M.; Mann, F.; Anderson, F.; Wood, M.; Jones, T.; Myers, D. Geochemical Processes Controlling Migration of Tank Wastes in Hanford's Vadose Zone. *Vadose Zone J.* **2007**, *6*, 985−1003.

(27) Ferrage, E.; Lanson, B.; Michot, L. J.; Robert, J. L. Hydration Properties and Interlayer Organization of Water and Ions in Synthetic Na-Smectite with Tetrahedral Layer Charge. Part 1. Results from X-Ray Diffraction Profile Modeling. *J. Phys. Chem. C* **2010**, *114*, 4515−4526.

Downloaded by SANDIA NATL LABORATORIES on September 13, 2015 | http://pubs.acs.org
Publication Date (Web): August 27, 2015 | doi: 10.1021/acs.jpcc.5b03253

DOI: 10.1021/acs.jpcc.5b03253
J. Phys. Chem. C 2015, 119, 20880−20891

Downloaded by SANDIA NATL LABORATORIES on September 13, 2015 | http://pubs.acs.org
Publication Date (Web): August 27, 2015 | doi: 10.1021/acs.jpcc.5b03253

(28) Ferrage, E.; Kirk, C. A.; Cressey, G.; Cuadros, J. Dehydration of Ca-Montmorillonite at the Crystal Scale. Part 2. Mechanisms and Kinetics. *Am. Mineral.* **2007**, *92*, 1007−1017.
(29) Liu, X. D.; Lu, X. C. A Thermodynamic Understanding of Clay-Swelling Inhibition by Potassium Ions. *Angew. Chem., Int. Ed.* **2006**, *45*, 6300−6303.
(30) Chavez-Paez, M.; dePablo, L.; dePablo, J. J. Monte Carlo Simulations of Ca-Montmorillonite Hydrates. *J. Chem. Phys.* **2001**, *114*, 10948−10953.
(31) Skipper, N. T.; Sposito, G.; Chang, F. R. C. Monte Carlo Simulation of Interlayer Molecular Structure in Swelling Clay Minerals. 2. Monolayer Hydrates. *Clays Clay Miner.* **1995**, *43*, 294−303.
(32) Shahriyari, R.; Khosravi, A.; Ahmadzadeh, A. Nanoscale Simulation of Na-Montmorillonite Hydrate under Basin Conditions, Application of CLAYFF Force Field in Parallel GCMC. *Mol. Phys.* **2013**, *111*, 3156−3167.
(33) Suter, J. L.; Sprik, M.; Boek, E. S. Free Energies of Absorption of Alkali Ions onto Beidellite and Montmorillonite Surfaces from Constrained Molecular Dynamics Simulations. *Geochim. Cosmochim. Acta* **2012**, *91*, 109−119.
(34) Oueslati, W.; Mefath, M.; Ben Rhaiem, H.; Ben Haj Amara, A. Cation Exchange Selectivity Versus Concentration of Competing Heavy Metal Cations (Pb^{2+},Zn^{2+}): Case of Na-Montmorillonite. *Phys. Procedia* **2009**, *2*, 1059−1063.
(35) Cygan, R. T.; Liang, J. J.; Kalinichev, A. G. Molecular Models of Hydroxide, Oxyhydroxide, and Clay Phases and the Development of a General Force Field. *J. Phys. Chem. B* **2004**, *108*, 1255−1266.
(36) Loewenstein, W. The Distribution of Aluminum in the Tetrahedra of Silicates and Aluminates. *Am. Mineral.* **1954**, *39*, 92−96.
(37) Guggenheim, S.; Koster van Groos, A. F. Baseline Studies of the Clay Minerals Society Source Clays: Thermal Analysis. *Clays Clay Miner.* **2001**, *49*, 433−443.
(38) Chiou, C. T. *Partition and Adsorption of Organic Contaminants in Environmental Systems*; Wiley-Interscience: Hoboken, NJ, 2002.
(39) Ferrage, E.; Tournassat, C.; Rinnert, E.; Lanson, B. Influence of pH on the Interlayer Cationic Composition and Hydration State of Ca-Montmorillonite: Analytical Chemistry, Chemical Modelling and XRD Profile Modelling Study. *Geochim. Cosmochim. Acta* **2005**, *69*, 2797−2812.
(40) Bourg, I. C.; Sposito, G. Molecular Dynamics Simulations of the Electrical Double Layer on Smectite Surfaces Contacting Concentrated Mixed Electrolyte (NaCl-$CaCl_2$) Solutions. *J. Colloid Interface Sci.* **2011**, *360*, 701−715.
(41) Greathouse, J. A.; Cygan, R. T. Water Structure and Aqueous Uranyl(VI) Adsorption Equilibria onto External Surfaces of Beidellite, Montmorillonite, and Pyrophyllite: Results from Molecular Simulations. *Environ. Sci. Technol.* **2006**, *40*, 3865−3871.
(42) Rotenberg, B.; Morel, J.-P.; Marry, V.; Turq, P.; Morel-Desrosiers, N. On the Driving Force of Cation Exchange in Clays: Insights from Combined Microcalorimetry Experiments and Molecular Simulation. *Geochim. Cosmochim. Acta* **2009**, *73*, 4034−4044.
(43) Teleman, O.; Jonsson, B.; Engstrom, S. A Molecular Dynamics Simulation of a Water Model with Intramolecular Degrees of Freedom. *Mol. Phys.* **1987**, *60*, 193−203.
(44) Plimpton, S. Fast Parallel Algorithms for Short-Range Molecular Dynamics. *J. Comput. Phys.* **1995**, *117*, 1−19.
(45) Martyna, G. J.; Tobias, D. J.; Klein, M. L. Constant-Pressure Molecular-Dynamics Algorithms. *J. Chem. Phys.* **1994**, *101*, 4177−4189.
(46) Parrinello, M.; Rahman, A. Polymorphic Transitions in Single-Crystals - A New Molecular-Dynamics Method. *J. Appl. Phys.* **1981**, *52*, 7182−7190.
(47) Shinoda, W.; Shiga, M.; Mikami, M. Rapid Estimation of Elastic Constants by Molecular Fynamics Dimulation under Constant Stress. *Phys. Rev. B: Condens. Matter Mater. Phys.* **2004**, *69*, 134103.
(48) Tuckerman, M. E.; Alejandre, J.; Lopez-Rendon, R.; Jochim, A. L.; Martyna, G. J. A Liouville-Operator Derived. Measure-Preserving Integrator for Molecular Dynamics Simulations in the Isothermal-Isobaric Ensemble. *J. Phys. A: Math. Gen.* **2006**, *39*, 5629−5651.
(49) Chang, F. R. C.; Skipper, N. T.; Sposito, G. Computer Simulation of Interlayer Molecular Structure in Sodium Montmorillonite Hydrates. *Langmuir* **1995**, *11*, 2734−2741.
(50) Martin, M. G. MCCCS Towhee: A Tool for Monte Carlo Molecular Simulation. *Mol. Simul.* **2013**, *39*, 1212−1222.
(51) Teich-McGoldrick, S. L.; Greathouse, J. A.; Cygan, R. T. Molecular Dynamics Simulations of Uranyl Adsorption and Structure on the Basal Surface of Muscovite. *Mol. Simul.* **2014**, *40*, 610−617.
(52) Berendsen, H. J. C.; Grigera, J. R.; Straatsma, T. P. The Missing Term in Effective Pair Potentials. *J. Phys. Chem.* **1987**, *91*, 6269−6271.
(53) Botan, A.; Rotenberg, B.; Marry, V.; Turq, P.; Noetinger, B. Hydrodynamics in Clay Nanopores. *J. Phys. Chem. C* **2011**, *115*, 16109−16115.
(54) Frenkel, D.; Smit, B. *Understanding Molecular Simulation: From Algorithms to Applications*, 2nd ed.; Academic Press: San Diego, 2002.
(55) Cases, J. M.; Berend, I.; Besson, G.; Francois, M.; Uriot, J. P.; Thomas, F.; Poirier, J. E. Mechanism of Adsorption and Desorption of Water-Vapor by Homoionic Montmorillonite 0.1. The Sodium-Exchanged Form. *Langmuir* **1992**, *8*, 2730−2739.
(56) Karaborni, S.; Smit, B.; Heidug, W.; Urai, J.; vanOort, E. The Swelling of Clays: Molecular Simulations of the Hydration of Montmorillonite. *Science* **1996**, *271*, 1102−1104.
(57) Meleshyn, A.; Bunnenberg, C. Swelling of Na/Mg-Montmorillonites and Hydration of Interlayer Cations: A Monte Carlo Study. *J. Chem. Phys.* **2005**, *123*, 074706.
(58) Berend, I.; Cases, J. M.; Francois, M.; Uriot, J. P.; Michot, L.; Masion, A.; Thomas, F. Mechanism of Adsorption and Desorption of Water-Vapor by Homoionic Montmorillonites 0.2. The Li^+, Na^+, K^+, Rb^+ and Cs^+-Exchanged Forms. *Clays Clay Miner.* **1995**, *43*, 324−336.
(59) Chiou, C. T.; Rutherford, D. W. Effects of Exchanged Cation and Layer Charge on the Sorption of Water and EGME Vapors on Montmorillonite Clays. *Clays Clay Miner.* **1997**, *45*, 867−880.
(60) Rutherford, D. W.; Chiou, C. T.; Eberl, D. D. Effects of Exchanged Cation on the Microporosity of Montmorillonite. *Clays Clay Miner.* **1997**, *45*, 534−543.
(61) Calvet, R. Hydration of Montmorillonite and Diffusion of Exchangeable Cations. 1. Hydration of Montmorillonite Saturated by Monovalent Cations. *Ann. Agron.* **1973**, *24*, 77−133.
(62) Fripiat, J. J.; Jelli, A.; Poncelet, G.; Andre, J. Thermodynamic Properties of Adsorbed Water Molecules and Electrical Conduction in Montmorillonites and Silicas. *J. Phys. Chem.* **1965**, *69*, 2185−2197.
(63) Posner, A. M.; Quirk, J. P. Changes in Basal Spacing of Montmorillonite in Electrolyte Solutions. *J. Colloid Sci.* **1964**, *19*, 798−812.
(64) Bishop, J. L.; Pieters, C. M.; Edwards, J. O. Infrared Spectroscopic Analyses on the Nature of Water in Montmorillonite. *Clays Clay Miner.* **1994**, *42*, 702−716.
(65) Laird, D. A. Layer Charge Influences on the Hydration of Expandable 2:1 Phyllosilicates. *Clays Clay Miner.* **1999**, *47*, 630−636.
(66) Sato, T.; Watanabe, T.; Otsuka, R. Effects of Layer Charge, Charge Location, and Energy Change on Expansion Properties of Dioctahedral Smectites. *Clays Clay Miner.* **1992**, *40*, 103−113.
(67) Suquet, H.; Malard, C.; Pezerat, H. Structure et Propriétés d'Hydratation des Nontronites. *Clay Miner.* **1987**, *22*, 157−167.
(68) Glaeser, R.; Mering, J. Ranges of Homogeneous Hydration in Smectites. *C. R. Acad. Sci. D Nat.* **1968**, *267*, 463−466.
(69) Burgess, J. *Ions in Solution: Basic Principles of Chemical Interactions*; Halsted Press: A Division of John Wiley & Sons: New York, NY, 1988.
(70) Marry, V.; Turq, P.; Cartailler, T.; Levesque, D. Microscopic Simulation of Structure and Dynamics of Water and Counterions in a Monohydrated Montmorillonite. *J. Chem. Phys.* **2002**, *117*, 3454−3463.
(71) Boek, E. S.; Coveney, P. V.; Skipper, N. T. Molecular Modeling of Clay Hydration: A Study of Hysteresis Loops in the Swelling Curves of Sodium Montmorillonites. *Langmuir* **1995**, *11*, 4629−4631.

DOI: 10.1021/acs.jpcc.5b03253
J. Phys. Chem. C 2015, 119, 20880−20891

(72) Hensen, E. J. M.; Smit, B. Why Clays Swell. *J. Phys. Chem. B* **2002**, *106*, 12664−12667.
(73) Tao, L.; Tian, X. F.; Yu, Z.; Tao, G. Swelling of K^+, Na^+ and Ca^{2+}-Montmorillonites and Hydration of Interlayer Cations: A Molecular Dynamics Simulation. *Chin. Phys. B* **2010**, *19*, 109101.
(74) Whitley, H. D.; Smith, D. E. Free Energy, Energy, and Entropy of Swelling in Cs-, Na-, and Sr-Montmorillonite Clays. *J. Chem. Phys.* **2004**, *120*, 5387−5395.
(75) Greathouse, J. A.; Hart, D. B.; Bowers, G. M.; Kirkpatrick, R. J.; Cygan, R. T. Molecular Simulation of Structure and Diffusion at Smectite−Water Interfaces: Using Expanded Clay Interlayers as Model Nanopores. *J. Phys. Chem. C* **2015**, *119*, 17126.
(76) Zang, J.; Nair, S.; Sholl, D. S. Osmotic Ensemble Methods for Predicting Adsorption-Induced Structural Transitions in Nanoporous Materials Using Molecular Simulations. *J. Chem. Phys.* **2011**, *134*, 184103.
(77) Hensen, E. J. M.; Tambach, T. J.; Bliek, A.; Smit, B. Adsorption Isotherms of Water in Li-, Na-,and K-Montmorillonite by Molecular Simulation. *J. Chem. Phys.* **2001**, *115*, 3322−3329.
(78) Ferrage, E.; Lanson, B.; Sakharov, B. A.; Drits, V. A. Investigation of Smectite Hydration Properties by Modeling Experimental X-ray Diffraction Patterns: Part I. Montmorillonite Hydration Properties. *Am. Mineral.* **2005**, *90*, 1358−1374.
(79) Hardin, E.; Hadgu, T.; Clayton, D.; Howard, R.; Greenberg, H.; Blink, J.; Sharma, M.; Sutton, M.; Carter, J.; Dupont, M.; Rodwell, P. Repository Reference Disposal Concepts and Thermal Management Analysis, FCRD-USED-2012−000219 Rev. 2; U.S. Department of Energy, Used Fuel Disposition R&D Campaign, 2012.

Downloaded by SANDIA NATL LABORATORIES on September 13, 2015 | http://pubs.acs.org
Publication Date (Web): August 27, 2015 | doi: 10.1021/acs.jpcc.5b03253

DOI: 10.1021/acs.jpcc.5b03253
J. Phys. Chem. C 2015, 119, 20880−20891